ADVANCED NANOBIOMED RESEARCH
www.advnanobiomedres.com

Esterase-Activatable and Glutathione-Responsive Triptolide Nano-Prodrug for the Eradication of Pancreatic Cancer

*Binglin Sui, Chen Cheng, Shanshan Shi, Mingming Wang, and Peisheng Xu**

Triptolide (TPL) is a small molecule isolated from a traditional Chinese herb *Tripterygium wilfordii* Hook F and shows excellent anticancer effect for pancreatic cancer cells. However, the poor water solubility and severe liver toxicity of TPL hindered its clinical application. Herein, TPL is covalently conjugated to a polymer and entrapped inside the core of the TPL nanogel (nTPL) to protect it from premature leakage during blood circulation. With the help of lactobionic acid (LBA), nTPL-LBA could selectively target the tumors in an orthotopic pancreatic cancer mouse model. TPL could be subsequently released intracellularly in its original form due to the presence of elevated intracellular esterase and GSH, and eventually kills cancer cells. nTPL-LBA treatment reduces tumor burden by 99% while not introducing TPL-associated liver and kidney toxicities. Most importantly, more than half of the nTPL-LBA-treated animals are tumor-free, suggesting that nTPL-LBA is an effective approach in eradicating pancreatic cancer.

1. Introduction

Pancreatic cancer is one of the most deadly malignancies to humans. The 5-year survival rate for pancreatic cancer is lower than 10%, which is the lowest among all types of cancers.[1] Compared with gemcitabine monotherapy, standard care of chemotherapy for pancreatic cancer, the newly developed combination therapy of gemcitabine and nab-paclitaxel only slightly improved the median survival from 6 to 7.8 months.[2] The dismal reality of pancreatic cancer treatment reveals the urgent need for therapeutic strategies with higher efficiency against pancreatic cancer.

Triptolide (TPL) is a bioactive diterpene triepoxide originated from a traditional Chinese medicinal herb *Tripterygium wilfordii* Hook F, commonly named as the thunder god vine or Lei Gong Teng in Chinese. It was found that TPL could exert a potent anticancer effect for many types of cancer, including pancreatic cancer, and thus it was considered as a promising chemotherapeutic option for malignant cancers.[3] However, the poor water solubility and severe liver toxicity of TPL hindered its potential clinical applications.[4] Various approaches have been utilized to improve its bioavailability and biocompatibility, including water-soluble TPL prodrug,[5] TPL-sugar conjugate,[6] TPL-aptamer conjugate,[7] TPL-peptide conjugate,[8] and TPL-encapsulated nanoparticles.[9] Among them, Minnelide, a hydrophilic prodrug of TPL, has effectively resolved the solubility problem of TPL and is currently being evaluated in clinical trials.[5] However, how to effectively eliminate the TPL-associated liver toxicity remains a challenge.[10]

The concept of "prodrug" generally refers to a masked and inactive form of a drug produced by reversible modification of the parent drug, which is conferred with more desirable physicochemical properties and is ready to be converted back to the bioactive form of the drug in vivo.[11] The prodrug strategy has been extensively explored to reduce the toxic side effects of many parent drugs.[12]

To improve the efficacy of an anticancer drug and reduce its side effects, drugs are frequently conjugated to a targeting ligand, which can bind to its corresponding receptors overexpressed in cancer cells. Research found that β-D-galactose receptors are overexpressed in a variety of cancer cells,[13] including pancreatic cancer.[14] Our previous study revealed that lactobionic acid (LBA), a disaccharide derivative composed of gluconic acid and galactose, could effectively binds to β-D-galactose receptors.[15] Herein, we developed a polymeric nano-prodrug system to circumvent the solubility issue of TPL and attenuate its toxicity through pancreatic cancer targeted delivery and intracellularly dual responsive release approaches (**Figure 1**). The cancer-targeted TPL nanoparticle (nTPL-LBA) exhibits outstanding efficacy in eradicating tumor in an orthotopic pancreatic cancer model while not inducing liver and kidney toxicity.

As shown in Figure 1A,B, the nano-prodrug (nTPL) of TPL is a polymeric nanogel prepared through crosslinking and self-assembly process of drug-conjugated polymers. TPL is attached to the PDA-PEG polymer, a copolymer of 2-(pyridin-2-yldisulfanyl)ethyl acrylate (PDA) and poly(ethylene glycol) methyl ether acrylate (PEG), via ester bonds which can be hydrolyzed to release the parent drug TPL (Scheme S1, Supporting

B. Sui, C. Cheng, S. Shi, M. Wang, P. Xu
Department of Drug Discovery and Biomedical Sciences
College of Pharmacy
University of South Carolina
715 Sumter St., Columbia, SC 29208, USA
E-mail: xup@cop.sc.edu

The ORCID identification number(s) for the author(s) of this article can be found under https://doi.org/10.1002/anbr.202100040.

© 2021 The Authors. Advanced NanoBiomed Research published by Wiley-VCH GmbH. This is an open access article under the terms of the Creative Commons Attribution License, which permits use, distribution and reproduction in any medium, provided the original work is properly cited.

DOI: 10.1002/anbr.202100040

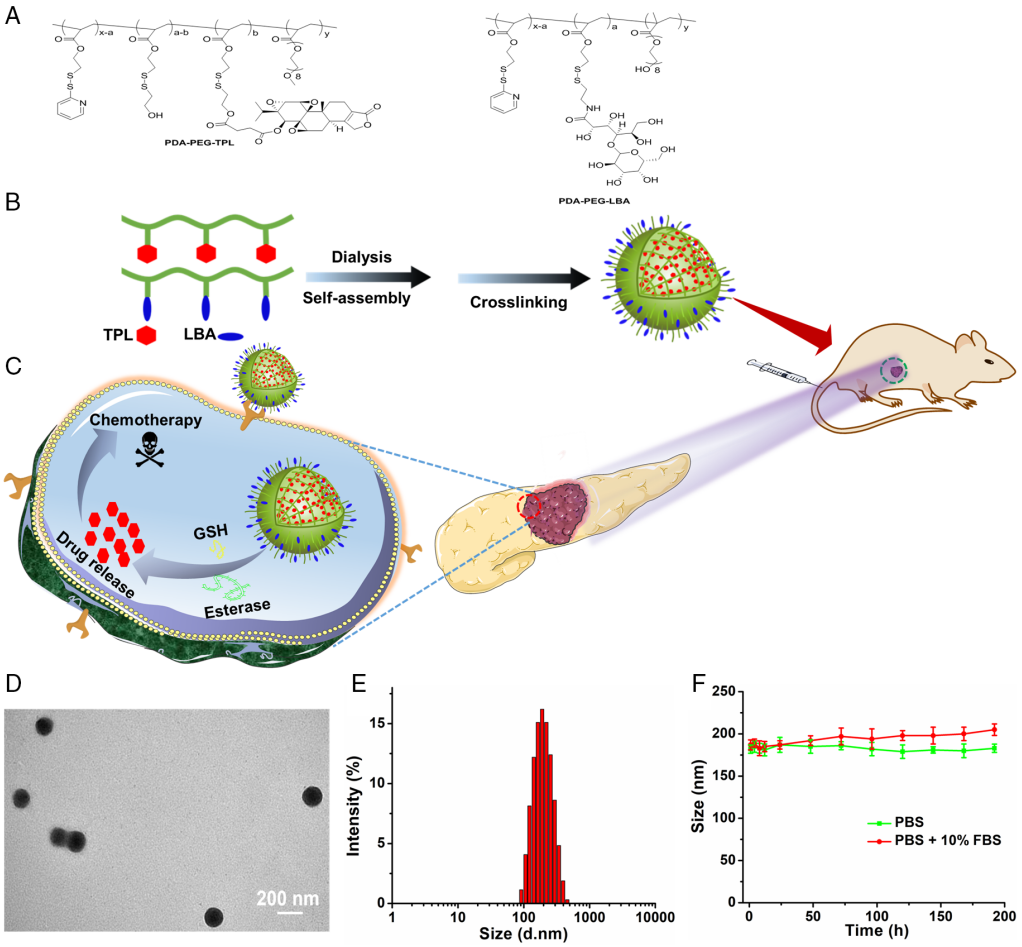


Figure 1. Schematic illustration of polymeric nanoprodrug nTPL-LBA for efficient intracellular delivery of anticancer drug TPL. A) The structures of PDA-PEG-TPL and PDA-PEG-LBA polymers. B) Fabrication of nTPL-LBA through a self-assembly and crosslinking process. C) β-D-galactose receptor-mediated cellular internalization of nTPL-LBA and the enzyme catalyzed on-demand release of TPL in tumor cells. D) TEM image of nTPL-LBA. E) Size distribution of nTPL-LBA. F) Colloidal stability of nTPL-LBA at different conditions. Data represent the means ± SD, $n = 3$.

Information). In addition to TPL, LBA is also incorporated in nTPL to yield targeted nTPL (nTPL-LBA) to guide the nano-prodrugs to the tumor sites and enter cancer cells.

When the nano-prodrug nTPL-LBA is fabricated in aqueous solution, the hydrophobic TPL will be encapsulated inside the nanogel, protecting it from premature leakage and thus minimizing its systemic toxicity, whereas the LBA moieties will be decorated on the surface of the nanogel thanks to its hydrophilic nature, making it convenient to target cancer cells (Figure 1). nTPL-LBA is expected to accumulate in the tumor via the so-called enhanced permeability and retention (EPR) effect,[16] and be taken up by cancer cells through receptor-mediated endocytosis, as shown in Figure 1C. The nTPL nanogel will be dissociated by chopping off the disulfide bonds with the elevated intracellular glutathione (GSH), whereas the ester bond linkage between TPL and the polymer chain will be cleaved with the help of the intracellular catalytic enzymes, esterases.[6] As a result, the cancer cells will be killed by the released TPL.

2. Results and Discussion

2.1. Fabrication and Characterization of TPL-Loaded Nanoparticle

To prepare the nTPL-LBA nanogel, TPL was first modified with succinic anhydride to yield TPL-SA.[6] TPL-SA was conjugated to PDA-PEG through an esterification reaction to produce polymer-drug conjugate of PDA-PEG-TPL (Scheme S1, Supporting Information). The chemical structures of these compounds were confirmed by nuclear magnetic resonance (NMR) spectroscopy (Figure S1–S3, Supporting information), and the content of TPL in the PDA-PEG-TPL was quantified to be 12.3% (w/w). A mixture of PDA-PEG-TPL and PDA-PEG-LBA in dimethyl sulfoxide (DMSO) was fabricated into micelles by dialysis in deionized water, and further crosslinked with the help of tris(2-carboxyethyl)phosphine (TCEP) to yield nTPL-LBA polymeric nanogels. As shown in Figure 1D, transmission electron microscopy (TEM) revealed that nTPL-LBA has a spherical morphology with a diameter of 154.7 ± 10.4 nm. Dynamic light scattering

© 2021 The Authors. Advanced NanoBiomed Research published by Wiley-VCH GmbH

(DLS) found that nTPL-LBA had a hydrodynamic size of 185.6 ± 8.8 nm with a dispersity of 0.10 ± 0.03 (Figure 1E), which is a little larger than its size in the dry state recorded by TEM. To verify the targeting ability of LBA, nontargeted nTPL nanogel was prepared from PDA-PEG-TPL polymer alone following the same procedure used for nTPL-LBA. TEM and DLS analysis showed that nTPL had similar morphology and size as those of nTPL-LBA (Figure S4–S6, Supporting Information). The zeta potential measurement showed that both nanogels had slightly negative charges on their surface (Figure S7, Supporting Information).

To serve as an outstanding targeted drug carrier, nTPL-LBA should have great stability during blood circulation. The colloidal stability of nTPL-LBA was examined by monitoring its hydrodynamic size with DLS in phosphate-buffered saline (PBS) (pH 7.4) and PBS supplemented with 10% fetal bovine serum (FBS). As shown in Figure 1F, no obvious size change observed in both conditions for nTPL-LBA, which makes it a suitable nano-prodrug for in vivo application.

2.2. The Release Kinetics of nTPL-LBA

High-performance liquid chromatography (HPLC) analysis revealed that the loading content (LC) and loading efficiency (LE) of TPL in nTPL-LBA were 11.5% and 98.9%, respectively. The TPL release profile of nTPL-LBA was investigated in varied conditions to mimic different physiological environments (**Figure 2**A). Little to a negligible amount (<5%) of TPL was released from the nano-prodrug in PBS (pH 7.4), PBS supplemented with 10% FBS or 2 mM GSH after 48 h of incubation. However, in the presence of 0.2 U mL^{-1} of esterase, which exists at a high level in the tumor tissue and intracellular environment and can catalyze the hydrolysis of ester bonds with high efficiency,[17] an accelerated release of TPL was observed. Interestingly, in an environment containing both esterase and 2 mM GSH, about 50% TPL was released within 10 h of incubation (Figure 2A). These results validate the drug release efficiency of nTPL-LBA and render it an ideal prodrug free of premature release before entering into cancer cells where the ester bond and disulfide linkers are cleaved by intracellular esterases and GSH, respectively.[6] HPLC and LC-MS analysis of the released products confirmed that the original form of TPL could be tracelessly released from the nanogel (Figure S8, S9, Supporting Information), which warrants the therapeutic efficacy of the nTPL-LBA nanogel.

2.3. Cellular Uptake of nTPL-LBA

To demonstrate the tumor-targeting ability of the LBA ligand in nTPL-LBA for pancreatic cancer, confocal laser scanning microscopy (CLSM) and flow cytometry (FCM) were utilized to evaluate the cellular uptake of nTPL and nTPL-LBA. PANC-1, a human pancreatic cancer cell line, was adopted for this research due to its less sensitivity to most anticancer drugs[18] and more resistance to TPL compared with prevailingly studied BXPC-3 cells (Figure S10, Supporting Information). PANC-1 cells were incubated with Cy3-labeled nTPL or nTPL-LBA, and then analyzed by

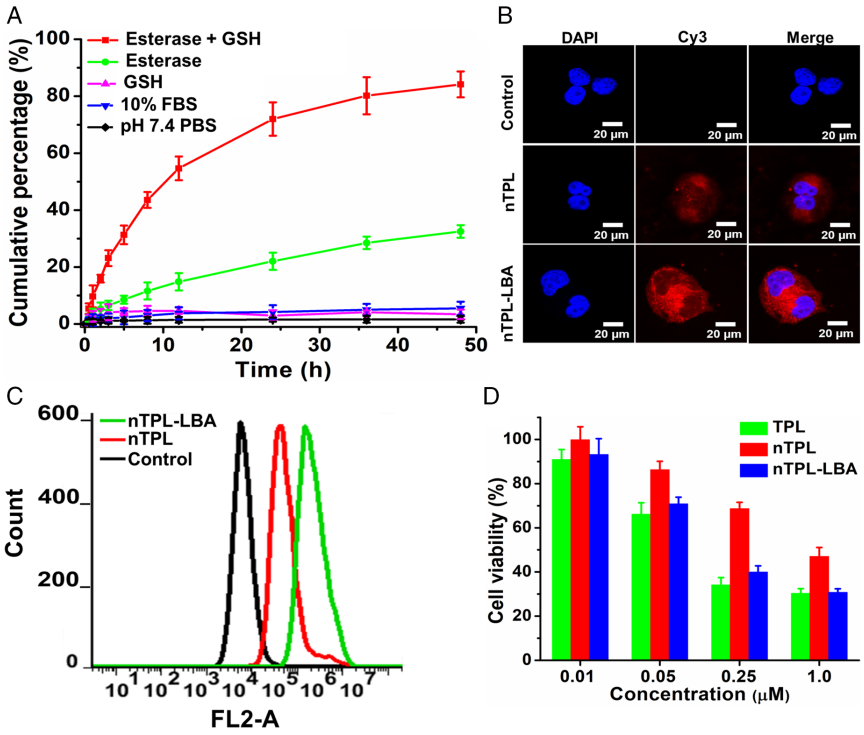


Figure 2. A) Drug release profiles of nTPL-LBA in different release media. The esterase and GSH concentrations used in the assay were 0.2 U mL^{-1} and 2 mM, respectively. B) Representative confocal fluorescence images of PANC-1/Luc cells after incubation with Cy3-labelled nTPL and nTPL-LBA for 3 h. Cell nuclei were stained with Hoechst 33342. C) Cellular internalization analysis of PANC-1/Luc cells after incubation with Cy3-labeled nTPL and nTPL-LBA for 3 h by flow cytometry. D) Cell viability of PANC-1/Luc cells after different treatments with TPL, nTPL, and nTPL-LBA for 72 h. Data represent the means ± SD, $n = 3$.

© 2021 The Authors. Advanced NanoBiomed Research published by Wiley-VCH GmbH

CLSM and FCM. As shown in Figure 2B, the relatively weak fluorescence (red) of Cy3 emitted from cells incubated with nTPL indicated that nTPL could be taken up by pancreatic cancer cells. In contrast, a much stronger fluorescence signal was observed in cells treated with nTPL-LBA, suggesting that more nTPL-LBA nanogels were taken up by the cells. The results of flow cytometry analysis (Figure 2C), which are in good agreement with the findings from CLSM, further verified the higher cellular uptake of nTPL-LBA nanogels. In addition, the preincubating of LBA significantly inhibited the cellular uptake of nTPL-LBA (Figure S11, Supporting Information) further validated that the improved uptake of nTPL-LBA was due to the β-D-galactose receptor-mediated endocytosis.

2.4. In Vitro Cytotoxicity

To test the anticancer efficacy of TPL and its nanogel counterparts, their in vitro cytotoxicity was evaluated in human pancreatic cancer PANC-1 cells using the 3-(4,5-dimethylthiazol-2-yl)-2,5-diphenyl tetrazolium bromide (MTT) assay at varying TPL equivalent concentrations. As shown in Figure 2D, both free TPL and the TPL nanogels exhibited anticancer activities in a dose-dependent manner as anticipated in a submicromolar level, confirming the high potency of TPL in killing pancreatic cancer cells. The IC_{50} of free TPL and nTPL were 66.1 and 145.8 nM, respectively. However, the LBA-modified nanogel, nTPL-LBA, exhibited a much higher potency in killing cancer cells, as evidenced by an IC_{50} of 69.5 nM, which is comparable with that of free TPL. This improved anticancer efficiency is ascribed to the enhanced cellular internalization of nTPL-LBA compared with nTPL, as shown in Figure 2B,C. Furthermore, the toxicity of the PDA-PEG polymer itself was negligible in the tested dose range (Figure S12, Supporting Information).

2.5. In Vivo Biodistribution of nTPL-LBA

Encouraged by the low premature release merit of nTPL-LBA and its high efficiency in killing cancer cell in vitro, we proposed to investigate the antitumor efficacy of the nanogels in vivo. An orthotopic pancreatic mouse tumor model was established

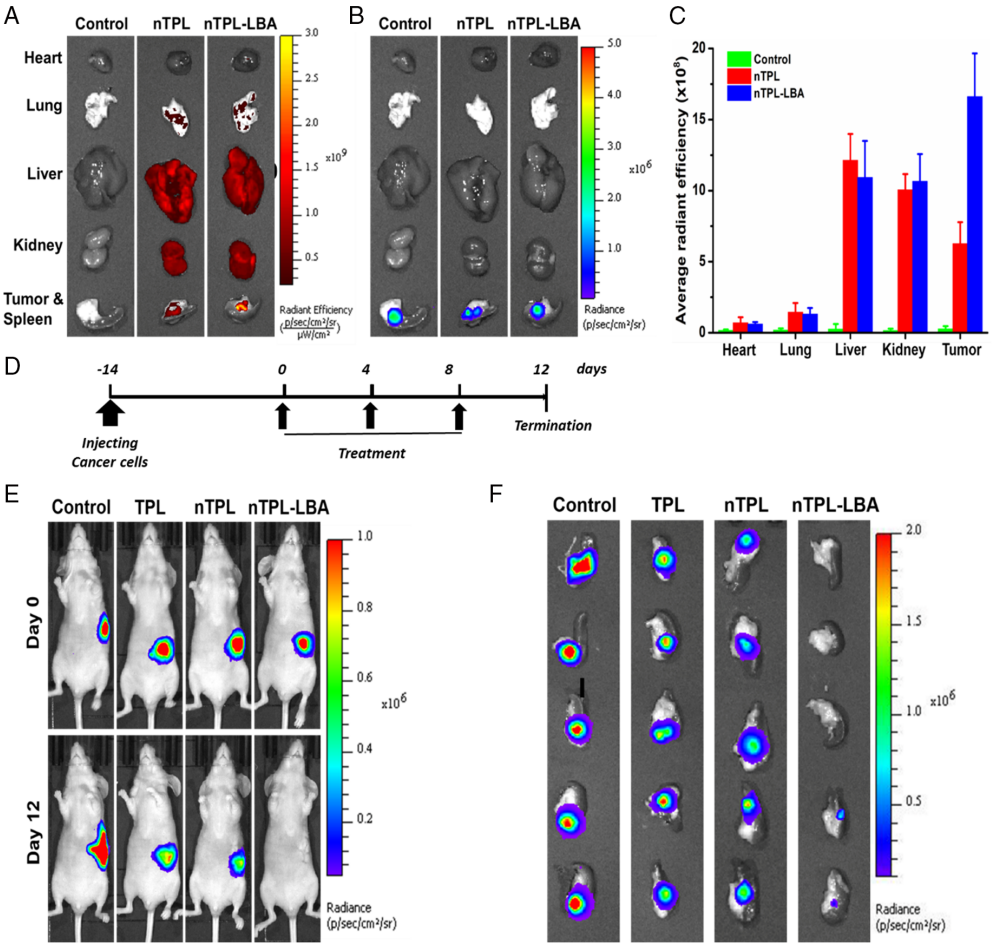


Figure 3. In vivo biodistribution and anticancer efficacy of the TPL nano-prodrugs in an orthotopic tumor mouse model of human pancreatic cancer. Ex vivo images acquired with a A) fluorescence filter and B) a luminescence filter. C) Quantitative analysis of mice organs and tumors after treatments with Cy3-labeled nano-prodrugs nTPL and nTPL-LBA. Data represent the means ± SD, $n = 3$. D) Treatment timeline for the tumor growth inhibitory assay. E) Representative whole body bioluminescence images of mice before and after treatments with free TPL and nanogels. F) Representative bioluminescence images of harvested pancreatic tumors attached to spleens from sacrificed mice.

© 2021 The Authors. Advanced NanoBiomed Research published by Wiley-VCH GmbH

as described in the literature.[19] PANC-1/Luc cells, which stably transfected with luciferase, were injected into the pancreatic tail of female nude mice through a laparotomy. As bioluminescence intensity is proportional to the population of cancer cells in the tumor,[13d] the size of a tumor was monitored via recording the intensity of bioluminescence emitted from the mice with a non-invasive IVIS imaging system after the injection of luciferin. The in vivo tumor targeting efficiency of the nanogels were investigated by detecting their biodistribution in tumor-bearing mice after i.v. injection of Cy3-labeled nanogels. As shown in **Figure 3**A,B, the fluorescence emission of Cy3 was mainly observed in tumors, kidneys, and livers of the mice. The excellent colocalization of fluorescence and bioluminescence signals in the tumor areas validated the tumor-specific accumulations of both nanogels due to the EPR effect. Figure 3C shows that the fluorescence intensity of tumors in mice treated with nTPL-LBA was twofold stronger than that detected in nTPL-treated mice, which confirmed the enhanced tumor targeting effect of nTPL-LBA. More importantly, the fluorescence signal in the nTPL-LBA treated group is the strongest among all collected organs (Figure 3C), suggesting its highly specific tumor targeting effect.

2.6. Tumor Growth Inhibitory Effect of nTPL-LBA

To investigate whether better tumor targeting effect of the nTPL-LBA nanogel could be translated into superior tumor growth inhibitory effect, orthotopic tumor-bearing mice were intravenously administrated with free TPL and nano-prodrugs at the TPL equivalent dose of 1.0 mg kg^{-1} through the tail vein at day 0, 4, and 8 (Figure 3D). As shown in Figure 3E, tumors treated with PBS in the control group grew rapidly, reflected by the much stronger bioluminescence signals detected in the pancreas region. Contrary to the control group, the weakened bioluminescence signals in free TPL and the TPL nanogel-treated mice, which validated that TPL and TPL nanogel were able to retard tumor growth and reduced the tumor burdens. To our surprise, almost no detectable signal was collected in the nTPL-LBA treated mice, suggesting the outstanding anticancer effect of nTPL-LBA nanogel.

To more accurately observe the tumor burden on the pancreas, pancreatic tumors attached to the spleen were harvested for further analysis. As shown in Figure 3F, tumors collected from the control group emitted very strong bioluminescence. In contrast, much weaker bioluminescence intensity was detected in the tumor from free TPL and nTPL nanogel-treated groups. For the five mice treated with nTPL-LBA, however, no detectable bioluminescence signal was collected in the pancreases of three mice, and only very weak signals were recorded from the pancreases of the remaining two animals.

The tumor burdens in different treatment groups were also monitored and quantitively recorded by an IVIS whole-body imaging system during the treatment (**Figure 4**A). As expected, a rapid increase of tumor burden, 4.3-fold, was observed in the control animals in the duration of 12 days. However, free TPL and nTPL gradually shrank the tumor burdens to 0.4-fold and 0.3-fold, respectively. Noteworthily, nTPL-LBA demonstrated the most potent antitumor efficacy, as evidenced by the sharply declined bioluminescence signal (Figure 4A). In addition, only a negligible ex vivo tumor signal was collected from the nTPL-LBA

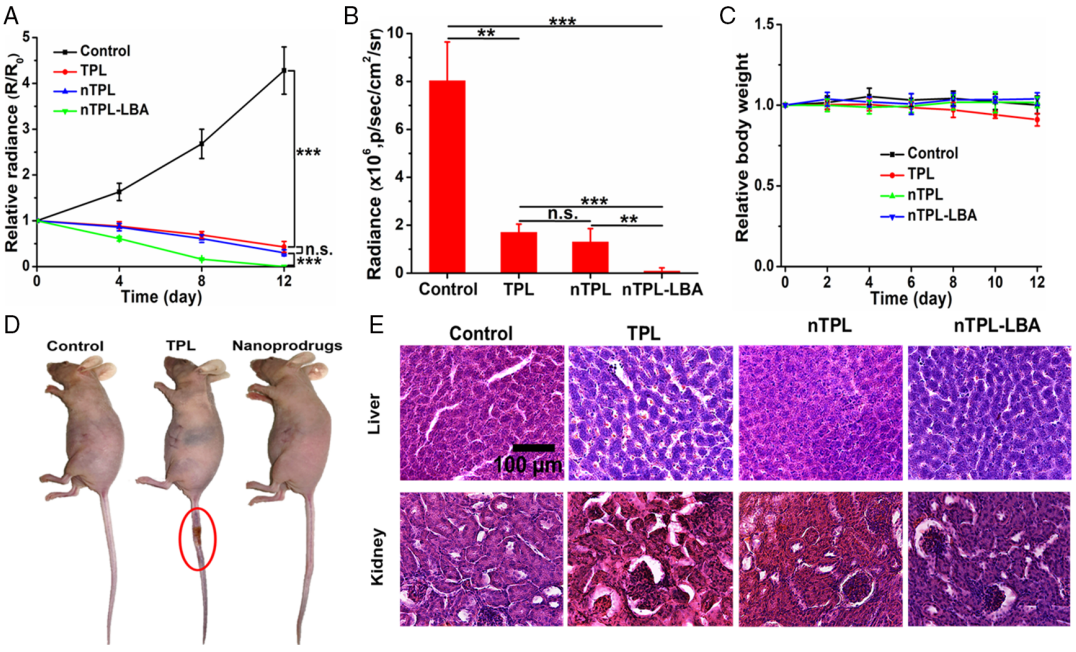


Figure 4. In vivo anticancer efficacy of the TPL nanogel in an orthotopic tumor mouse model of human pancreatic cancer. A) Bioluminescent intensity of the mice at predetermined time points. B) Quantitative analysis of harvested pancreatic tumors attached to spleens from sacrificed mice. C) Body weight change of mice during the experiment. D) Body pictures of mice after the last treatment. The red circle highlights the irritation area on the tail skin of mice treated with free TPL. E) H&E staining of liver and kidney tissues from mice in different treatment groups. Data represent the means ± SD, $n = 5$. $^{**}P < 0.01$ and $^{***}P < 0.001$; n.s.: no significance.

© 2021 The Authors. Advanced NanoBiomed Research published by Wiley-VCH GmbH

group (Figure 4B), as supported by 99% tumor burden reduction. These observations collectively confirmed the outstanding anticancer efficacy of nTPL-LBA and implied that nTPL-LBA is a powerful tool for eradicating pancreatic cancer.

2.7. Systemic Toxicity of nTPL-LBA

As mentioned earlier, in addition to the poor solubility in aqueous media, the systemic toxicity of TPL is another obstacle for its clinical application. Mice in the free TPL group showed a trend of body weight loss (Figure 4C), whereas no noticeable body weight loss was observed throughout the whole period of experiment in mice in other treatment groups. In addition, there are signs of swelling and necrosis in the tail skin of the mice treated with free TPL (Figure 4D), whereas no similar tissue damage was observed in both nTPL and nTPL-LBA nanogel-treated groups. These results demonstrated that the nano-prodrug strategy could effectively circumvent the destructive side effects induced by TPL. To further evaluate the systemic toxicity of free TPL and TPL nanogels, the major organs collected from sacrificed mice were analyzed by hematoxylin and eosin (H&E) staining. There was no difference between control and treatment groups in the heart and spleen tissues (Figure S13, Supporting Information). However, as shown in Figure 4E, the liver tissues of mice receiving free TPL treatment exhibited serious vacuolar degeneration and swollen cells, typical hepatotoxicity of free TPL. As expected, no obvious liver injury was found in nTPL-treated mice, and only some very mild abnormality was observed in the mice treated with nTPL-LBA. In addition, the kidney tissues from the animals treated with free TPL also showed minor renal damage, whereas no sign of similar renal toxicity was observed in other treatment groups (Figure 4E). These results proved that, through the nano-prodrug design, the severe systemic toxicity of TPL could be efficiently attenuated.

3. Conclusion

In summary, a highly efficient nano-prodrug nTPL-LBA was developed for targeted delivery and controlled release of a natural compound TPL for pancreatic cancer treatment. Due to its hydrophobic property, TPL moieties were entrapped inside the core of the nanogel, protecting them from premature leakage during blood circulation. With the help of LBA, a tumor-targeting ligand for pancreatic cancer cells, nTPL-LBA could be selectively targeted to the tumors in an orthotopic pancreatic cancer mouse model and being internalized by cancer cells. TPL will be subsequently released inside the cells due to the presence of elevated intracellular esterase and GSH, and eventually kills cancer cells. Consequently, the nTPL-LBA nanogel could effectively eradicate pancreatic tumors while not introducing TPL-associated liver and kidney toxicities. This intracellular releasing and nano-prodrug strategy opens a new window for the application of highly toxic while potent drugs in cancer therapy.

4. Experimental Section

Chemicals: *N*-(3-dimethylaminopropyl)-*N*′-ethylcarbodiimide hydrochloride (EDC), *N*,*N*′-dicyclohexylcarbodiimide (DCC), 2,2'-dipyridyl disulfide, MTT, silica gel (spherical, 100 μm), triethylamine (TEA), and TCEP were all purchased from Tokyo Chemical Industry Co., Ltd (Portland, OR, USA). Acryloyl chloride, 2,2′-azobis(2-methylpropionitrile) (AIBN), cystamine dihydrochloride, *N*,*N*-diisopropylethylamine (DIPEA), 4-(dimethylamino)pyridine (DMAP), glacial acetic acid, *N*-hydroxysuccinimide (NHS), LBA, 2-mercaptoethanol (BME), PBS, poly(ethylene glycol) methyl ether acrylate (PEGMEA, average Mn = 480 Da), porcine liver esterase (PLE), and succinic anhydride were all purchased from Sigma-Aldrich Chemical Co. (St. Louis, MO, USA). TPL was purchased from Aktin Chemicals, Inc. (Chengdu, China). Potassium D-luciferin (XenoLight) was purchased from PerkinElmer, Inc. (Waltham, MA, USA). FBS, Dulbecco's modified Eagle's medium (DMEM, Gibco), Hoechst 33342 (Invitrogen), penicillin–streptomycin (PS), and trypsin-EDTA were purchased from Thermo Fisher Scientific, Inc. (Waltham, MA, USA). Deuterated chloroform was purchased from Cambridge Isotope Laboratories, Inc. (Andover, MA, USA), and the other solvents used in all the experiments were purchased from Sigma-Aldrich Chemical Co. (St. Louis, MO, USA). The PDA-PEG polymer was synthesized according to our published protocol through free radical polymerization.[12] Gel permeation chromatography revealed that the polymer has a molecular weight of 27.8 kDa with a PDI of 1.37. Polymers PDA-PEG-BME[12] and PDA-PEG-LBA[15b] were prepared following our previously reported procedures.

Synthesis of PDA-PEG-TPL: Starting with commercial TPL, succinic acid modified TPL (TPL-SA) was synthesized in one step as described in the literature (Scheme S1, Supporting Information).[6] TPL was conjugated to the polymer via an esterification reaction between the carboxylic acid group of TPL-SA and the hydroxyl group of PDA-PEG-BME. To a solution of PDA-PEG-BME (20 mg) in DCM (500 μL), TPL-SA (3.3 mg), DCC (2.9 mg), and DMAP (0.9 mg) were added. The reaction mixture was filtered after stirring in the dark for 24 h at room temperature. The filtrate was diluted with DMSO (1 mL) and dialyzed against DMSO for 48 h using a Spectra/Por dialysis tube (MWCO: 8 kDa) to remove small molecules. Then DMSO was exchange into water through dialysis toward deionized water. The product PDA-PEG-TPL was obtained through lyophilization in the dark (19 mg, 82%). The chemical structure of the polymer PDA-PEG-TPL was verified by ^{1}H NMR and the content of TPL was determined with HPLC (Agilent 1260 Infinity II, Kinetex C18-column (50 × 2.1 mm^2, particle size 5 μm), solvent: 35% water (containing 0.1% trifluoroacetic acid) + 10% acetonitrile + 55% methanol, flow rate 0.5 mL min^{-1}, detection: 240 nm, elution time: 30 min, retention time : 2.5 min. ^{1}H NMR (300 MHz, $CDCl_3$) δ 8.45 (s), 7.69 (s), 7.11 (s), 5.07 (s), 4.67 (s), 4.32 (s), 4.17 (s), 3.83 (s), 3.64 (s), 3.54 (t), 3.37 (s), 3.03 (s), 2.90 (s), 2.75–2.70 (m), 2.34 (s), 2.14 (s), 1.93–1.89 (m), 1.67–1.59 (m), 1.05–0.80 (m).

Fabrication of Nano-Prodrugs: Polymer nano-prodrugs were fabricated through TCEP-induced crosslinking approach following our previously reported procedures.[12] Briefly, TCEP (0.3 mg) in DMSO (20 μL) was added to a DMSO solution (0.5 mL) of PDA-PEG-TPL polymer (or a polymer mixture of PDA-PEG-TPL and PDA-PEG-LBA at the ratio of 5:1 w/w, 10 mg) under robust stirring. 15 min later, the resulted polymer solution was dispersed dropwise into deionized water (5 mL) upon vigorous stirring to assemble into polymeric nanogels and stirred overnight. Then the polymeric nanogels were purified through dialysis against PBS (pH 7.4) in Spectra/Por dialysis tube (MWCO: 8 kDa) for 24 h. The final nano-prodrugs were stored at 4 °C for use. The zeta potential, hydrodynamic size, and distribution of the nano-prodrugs were analyzed by dynamic light scattering (DLS), recorded on Zetasizer (Zetasizer Nano ZS, Malvern Instruments Ltd., Malvern, UK). DLS and zeta-potential measurements were carried out in PBS (pH 7.4) at the concentration of 1.0 mg mL^{-1}. The physical morphology was measured by Hitachi HT7800 TEM (Hitachi High-Technologies Corporation, Tokyo, Japan). The content of TPL in the nano-prodrugs was determined by HPLC, and the LC and LE of TPL were calculated by the following equations.

$$\mathrm{LC}\,(\%) = \frac{\text{weight of TPL in nano}}{\text{weight of the nano}} \times 100\% \quad (1)$$

© 2021 The Authors. Advanced NanoBiomed Research published by Wiley-VCH GmbH

$$\text{LE}\,(\%) = \frac{\text{weight of TPL in nano}}{\text{weight of TPL feed}} \times 100\% \quad (2)$$

Serum Stability Assay: The colloidal stability of the nano-prodrugs was analyzed by DLS. The nano-prodrugs dispersed in PBS (pH 7.4) and PBS (pH 7.4) containing 10% FBS at the concentration of 1.0 mg mL^{-1} supplemented with sodium azide (0.01% w/v) were incubated at 37 °C for 8 days, and the size of the nano-prodrugs was monitored by DLS at different time points.

Drug Release: The drug release of TPL from nano-prodrug nTPL was investigated at 37 °C with PBS (pH 7.4) in the presence or absence of 10% FBS, 0.2 U mL^{-1} esterase, 2 mM GSH, or both 0.2 U/mL esterase and 2 mM GSH as release media. Nano-prodrugs dispersed in release media were quickly sealed in Spectra/Por dialysis tube (MWCO: 8 kDa) and instantly immersed into prewarmed release media (100 mL). Release media was sampled (10 mL per sample) at predesigned time points and fresh release media were replaced to keep the volume of the entire release systems constant. The collected samples were lyophilized to remove the aqueous media and the residues were dissolved into acetonitrile for analysis with HPLC.

Cell Culture: Human pancreatic cancer cells, PANC-1/Luc cells (a luciferase-expressing cell line derived from PANC-1, kindly donated by Dr. Erica Sloan at Monash University), were cultured in Gibco DMEM supplemented with 100 μg mL^{-1} streptomycin, 100 units mL^{-1} penicillin, and 10% FBS under a humidified atmosphere of 5% CO_2 at 37 °C. Cells were subcultured when the cell confluence attained about 80%.

Cytotoxicity Assay: The anticancer effect of the nano-prodrugs against PANC-1/Luc cells were investigated by MTT assay. Cells seeded in 96-well plates (5000 cells/well) were cultured at 37 °C with 5% CO_2 24 h before the test. Then cells were incubated with free TPL or nano-prodrugs at varied concentrations of TPL for 72 h. TPL was dissolved into DMSO and then diluted with fresh medium to the desired concentrations for MTT assay. Cells were allowed to grow with no incubation in the control group. After the removal of incubation medium, MTT reagent dissolved in fresh medium (100 μL) was added to each well (final concentration 1 mg mL^{-1}), and cells were incubated for another 4 h. MTT stop solution (100 μL) was added to dissolve the formed MTT crystal, and the optical density at 595 nm was measured by a microplate reader.

Cellular Uptake Observed by Confocal Microscopy: The cellular uptake of nano-prodrugs was studied in PANC-1/Luc cells with confocal fluorescence microscopy. Cells cultured in 35 mm^2 glass-bottom Petri dish (200 000 cells/dish) for 24 h were washed with PBS, and then treated with Cy3-labeled nano-prodrugs, nTPL, and nTPL-LBA, for 3 h. To validate that nTPL-LBA entering PANC-1 cell through the β-D-galactose receptor-mediated endocytosis, free LBA (1 mg mL^{-1}) was added to the medium before the addition of nTPL-LBA nanoparticles. In the control group, cells were treated with only medium. Subsequently, cells were washed with PBS for three times and fixed with 4% paraformaldehyde (PFA) for 10 min. After removal of PFA, cells were stained with Hoechst 33342 at a concentration of 1 μg mL^{-1} for 10 min. Then the staining solution was removed, and cells were imaged with a confocal fluorescence microscope (LSM 700, Carl-Zeiss Inc.).

Flow Cytometry Analysis: The cellular uptake of nano-prodrugs by PANC-1/Luc cells was also investigated with flow cytometry. Cells cultured in six-well plates (300 000 cells/well) for 24 h were washed with PBS, and then treated with Cy3-labeled nano-prodrugs for 3 h. In the control group, cells were treated with only medium. Cells were then trypsinized with trypsin–EDTA and centrifuged at 2000 rpm for 3 min. The collected cell pellets were washed with PBS via centrifuging for another two times. At last, cell pellets were resuspended into PBS, and the intracellular fluorescence intensity of cells was measured by flow cytometry (BD Accuri C6, BD Biosciences).

Animal Model Establishment: All the experiments involving animals were performed in accordance with NIH regulations, and the experimental protocols were approved by the Institutional Animal Care and Use Committee of the University of South Carolina (protocol #: 2425-101350-082718). An orthotopic pancreatic tumor mouse model was established as described in the literature.[19] Briefly, PANC-1/Luc cells cultured in DMEM were trypsinized with trypsin-EDTA and collected via centrifuging at 2000 rpm for 3 min. 2 000 000 cells were dispersed in 20 μL ice-cold mixture of PBS and Matrigel (2:3, v/v). Mice were first anesthetized with isoflurane, and then a 1 cm incision was made in the abdominal skin and underlying muscle to expose the entire pancreas together with spleen. The cell suspension was slowly injected into the pancreas through the tail of the pancreas using a 29 G 0.3 mL insulin syringe. The syringe was held still in the pancreas for 1 min for the Matrigel to get solidified, and then the needle was gently removed from the pancreas. The spleen and pancreas were carefully returned back to the abdominal cavity, and the abdominal musculature and external skin were sequentially closed with an absorbable braided 4-0 suture and a nonabsorbable monofilament 6-0 suture, respectively. Each mouse was subcutaneously injected with 0.1 mg kg^{-1} buprenorphine as an analgesic after surgery. Ten days after the surgery, the external sutures were removed from the mice. The tumor burdens in mice were monitored with an IVIS Lumina III imaging system (PerkinElmer Inc., Waltham, USA), and the body weight of animals and signs of pain were monitored throughout the entire experiment process.

Whole Body Imaging: The growth of tumor burdens was detected with the IVIS Lumina III imaging system. In brief, nude mice bearing orthotopic PANC-1/Luc tumors were anesthetized with isoflurane and intraperitoneally administrated with 15 mg mL^{-1} D-luciferin (200 μL). 15 min later, the mice were imaged and the bioluminescence signals of PANC-1/Luc tumors were recorded. All the bioluminescence images were taken with the same system settings. The images were processed with Living Image software and the bioluminescence intensity of images was analyzed in radiance.

In Vivo Biodistribution: After inoculation with PANC-1/Luc cells for 3 weeks, the mice were intravenously injected with Cy3-labeled nano-prodrugs, nTPL and nTPL-LBA, at a Cy3 equivalent dose of 1 mg kg^{-1}. Mice injected with PBS were used as control. All the mice were sacrificed at 6 h after the injection. The tumors and organs of mice were harvested for ex vivo imaging with the IVIS Lumina III imaging system through both the fluorescence and the bioluminescence channels.

Antitumor Efficacy: Two weeks after the surgery of PANC-1/Luc tumor inoculation, the mice bearing tumors were assigned into six groups with five mice in each group randomly. Free TPL was dissolved into a mixture of DMSO and Cremophor EL (1:1 v v^{-1}) at 5 mg mL^{-1} a d then diluted with PBS to a desired concentration. Animals were intravenously administrated with TPL or nano-prodrugs, nTPL and nTPL-LBA, at a TPL equivalent dose of 1 mg kg^{-1}. PBS was administrated in the control group. The treatments were administrated to the animals once every four days. Twelve days after the start of the treatment, all the mice were sacrificed to harvest the tumors and organs for further analysis.

Histological Analysis: The organs collected from mice were first fixed with 4% PFA in PBS (pH 7.4) at 4 °C for 24 h, and then embedded in optimal cutting temperature (OCT). These information have been added to the histological analysis method. The sections of embedded organs with a thickness of ≈10 μm were analyzed under a light microscope after H&E staining using the magnification of 10× and 40×. The histology was carried out in a blinded fashion by professional personnel at the University of South Carolina.

Statistical Analysis: The results were analyzed and expressed as the mean ± standard deviations. Student's two-tailed *t*-test was used to determine statistical significance ($P < 0.05$) between parallel groups.

Supporting Information

Supporting Information is available from the Wiley Online Library or from the author.

Acknowledgements

B.S., C.C., and P.X. contributed equally to this work. The authors thank National Institutes of Health (1R01AG054839-01A1, 1R41CA254500-01A1, and 1R21CA252360-01) for the financial support of the research.

© 2021 The Authors. Advanced NanoBiomed Research published by Wiley-VCH GmbH

Conflict of Interest

The authors declare no conflict of interest.

Data Availability Statement

Research data are not shared.

Keywords

esterase-activatable, intracellular releases, nano-prodrug, pancreatic cancer, triptolide

Received: March 15, 2021
Revised: May 27, 2021
Published online: August 2, 2021

[1] a) R. L. Siegel, K. D. Miller, A. Jemal, *CA: A Cancer J. Clin.* **2019**, *69*, 7; b) C. L. Wolfgang, J. M. Herman, D. A. Laheru, A. P. Klein, M. A. Erdek, E. K. Fishman, R. H. Hruban, *CA: Cancer J. Clin.* **2013**, *63*, 318.

[2] a) E. Borazanci, D. D. Von Hoff, *Expert Rev. Gastroenterol. Hepatol.* **2014**, *8*, 739; b) D. D. Von Hoff, T. Ervin, F. P. Arena, E. G. Chiorean, J. Infante, M. Moore, T. Seay, S. A. Tjulandin, W. W. Ma, M. N. Saleh, M. Harris, M. Reni, S. Dowden, D. Laheru, N. Bahary, R. K. Ramanathan, J. Tabernero, M. Hidalgo, D. Goldstein, E. Van Cutsem, X. Wei, J. Iglesias, M. F. Renschler, *N. Engl. J. Med.* **2013**, *369*, 1691.

[3] a) P. A. Phillips, V. Dudeja, J. A. McCarroll, D. Borja–Cacho, R. K. Dawra, W. E. Grizzle, S. M. Vickers, A. K. Saluja, *Cancer Res.* **2007**, *67*, 9407; b) X. Shi, Y. Jin, C. Cheng, H. Zhang, W. Zou, Q. Zheng, Z. Lu, Q. Chen, Y. Lai, J. Pan, *Clin. Cancer Res.* **2009**, *15*, 1686; c) D. V. Titov, B. Gilman, Q.-L. He, S. Bhat, W.-K. Low, Y. Dang, M. Smeaton, A. L. Demain, P. S. Miller, J. F. Kugel, J. A. Goodrich, J. O. Liu, *Nat. Chem. Biol.* **2011**, *7*, 182.

[4] a) Z.-L. Zhou, Y.-X. Yang, J. Ding, Y.-C. Li, Z.-H. Miao, *Nat. Prod. Rep.* **2012**, *29*, 457; b) Z.-y. Hou, X.-p. Tong, Y.-b. Peng, B.-k. Zhang, M. Yan, *Biomed. Pharmacother.* **2018**, *104*, 771.

[5] S. Banerjee, A. Saluja, *Pancreatology* **2015**, *15*, S39.

[6] Q.-L. He, I. Minn, Q. Wang, P. Xu, S. A. Head, E. Datan, B. Yu, M. G. Pomper, J. O. Liu, *Angew. Chem., Int. Ed.* **2016**, *55*, 12035.

[7] B. Liu, B. Guo, X. He, G. Zhang, A. Lu, *Mol. Ther.* **2014**, *22*, S221.

[8] T. Tian, Y. Song, K. Li, Y. Sun, Q. Wang, *Mol. Pharmaceut.* **2018**, *15*, 560.

[9] a) D. Ling, H. Xia, W. Park, M. J. Hackett, C. Song, K. Na, K. M. Hui, T. Hyeon, *ACS Nano* **2014**, *8*, 8027; b) C. Wang, B. Liu, X. Xu, B. Zhuang, H. Li, J. Yin, M. Cong, W. Xu, A. Lu, *Oncotarget* **2016**, *7*, 8360.

[10] H. Xu, B. Liu, *Eur. J. Med. Chem.* **2019**, *164*, 342.

[11] a) A. G. Cheetham, R. W. Chakroun, W. Ma, H. Cui, *Chem. Soc. Rev.* **2017**, *46*, 6638; b) V. Taresco, C. Alexander, N. Singh, A. K. Pearce, *Adv. Ther.* **2018**, *1*, 1800030; c) R. Walther, J. Rautio, A. N. Zelikin, *Adv. Drug Deliv. Rev.* **2017**, *118*, 65.

[12] B. Sui, C. Cheng, M. Wang, E. Hopkins, P. Xu, *Adv. Funct. Mater.* **2019**, *29*, 1906433.

[13] a) P. García Calavia, I. Chambrier, M. J. Cook, A. H. Haines, R. A. Field, D. A. Russell, *J. Colloid Interface Sci.* **2018**, *512*, 249; b) Z. Wang, P. Wu, Z. He, H. He, W. Rong, J. Li, D. Zhou, Y. Huang, *J. Mater. Chem. B* **2017**, *5*, 7591; c) L. Zhang, Y. Chen, Z. Li, L. Li, P. Saint-Cricq, C. Li, J. Lin, C. Wang, Z. Su, J. I. Zink, *Angew. Chem. Int. Ed.* **2016**, *55*, 2118; d) H. He, E. Markoutsa, J. Li, P. Xu, *Acta Biomater.* **2018**, *68*, 113.

[14] a) A. J. Gunn, Y. Hama, Y. Koyama, E. C. Kohn, P. L. Choyke, H. Kobayashi, *Cancer Sci.* **2007**, *98*, 1727; b) T. Arumugam, V. Paolillo, D. Young, X. Wen, C. D. Logsdon, L. De Palatis, M. M. Alauddin, *Nucl. Med. Biol.* **2014**, *41*, 833; c) L. G. Flores, S. Bertolini, H. H. Yeh, D. Young, U. Mukhopadhyay, A. Pal, Y. Ying, A. Volgin, A. Shavrin, S. Soghomonyan, W. Tong, W. Bornmann, M. M. Alauddin, C. Logsdon, J. G. Gelovani, *PloS ONE* **2009**, *4*, 7977.

[15] H. He, E. Markoutsa, J. Li, P. Xu, *Acta Biomater* **2018**, *68*, 113.

[16] a) M. Overchuk, G. Zheng, *Biomaterials* **2018**, *156*, 217; b) S. Wang, G. Yu, Z. Wang, O. Jacobson, R. Tian, L.-S. Lin, F. Zhang, J. Wang, X. Chen, *Adv. Mater.* **2018**, *30*, 1803926; c) H. Maeda, *J. Control. Release* **2012**, *164*, 138.

[17] a) C. Höllerer, G. Becker, T. Göen, E. Eckert, *Toxicol. In Vitro* **2018**, *47*, 178; b) K. Okada, T. Yamaguchi, K. Dodo, M. Sodeoka, S. Obika, *Bioorg. Med. Chem.* **2019**, *27*, 1444.

[18] N. Awasthi, C. H. Zhang, A. M. Schwarz, S. Hinz, C. G. Wang, N. S. Williams, M. A. Schwarz, R. E. Schwarz, *Carcinogenesis* **2013**, *34*, 2361.

[19] M. G. Chai, C. Kim-Fuchs, E. Angst, E. K. Sloan, *J. Vis. Exp.* **2013**, *76*, e50395.

© 2021 The Authors. Advanced NanoBiomed Research published by Wiley-VCH GmbH